Korea-Australia Rheology Journal, 30(3), 147-159 (August 2018) www.springer.com/13367
DOI: 10.1007/s13367-018-0015-9

Nonlinear viscoelastic behavior of aqueous foam under large amplitude oscillatory shear flow

Badri Vishal* and Pallab Ghosh
Department of Chemical Engineering, Indian Institute of Technology Guwahati, Guwahati 781039, India
(Received September 30, 2017; final revision received April 13, 2018; accepted April 24, 2018)

Aqueous foams are dispersions of gas bubbles in water, stabilized by surfactant, and sometimes particles. This multiphasic composition gives rise to complex rheological behavior under deformation. Understanding this behavior is important in many applications. Foam shows nonlinear rheological behavior at high deformation, which can be investigated by the large amplitude oscillatory shear (LAOS) experiments. In the present work, we have performed a systematic LAOS study of foam stabilized by 0.1 mol m^{-3} hexadecyltrimethylammonium bromide and 0.5 wt.% silica nanoparticles. The Lissajous-Bowditch curves and stress waveforms were analyzed at various strain amplitudes. These curves were fitted by Fourier transform rheology and Chebyshev polynomials to understand the contribution of the higher harmonic terms in LAOS. The intracycle LAOS behavior was explained based on the sequence of physical processes. The foam exhibited intracycle strain-hardening and shear-thinning at high deformation. Shear-thickening behavior was observed at moderate deformations.

Keywords: Chebyshev polynomial, foam, Fourier-transform rheology, large amplitude oscillatory shear, Lissajous-Bowditch curve, nonlinear viscoelasticity

1. Introduction

Aqueous foams are soft complex materials, which show viscoelastic behavior and possess an apparent yield stress. The rheology of these foams is of great interest in the production of cosmetics and foods, oil recovery, and minerals separation (Ahmadi *et al.*, 2015; Denkov *et al.*, 2009; Dickinson, 2015; Höhler and Cohen-Addad, 2005; Labiausse *et al.*, 2007). When an oscillatory shear strain is imposed below its yield value, foams exhibit solid-like behavior as the storage modulus (G') is greater than the loss modulus (G'') (Balmforth *et al.*, 2014). Upon increasing the strain amplitude (γ_0), a nonlinear viscoelastic response sets in. A detailed study of a linear viscoelastic behavior of foams has been reported elsewhere (Rouyer *et al.*, 2005; Saint-Jalmes and Durian, 1999). Princen (1982) and Khan and Armstrong (1986) have correlated the stress-response with the morphology of the foams by considering a two-dimensional network model. This can also be studied by simulating the foams based on their geometry using a two- or three-dimensional model (Tammaro *et al.*, 2016). Various methods have been proposed to study nonlinear viscoelastic properties of foams. Steady shear flow has been used to study the nonlinear behavior of foams (Denkov *et al.*, 2008). When the foam is sheared below its yield value, the angle between the foam films still remains $2\pi/3$ rad, as per the Plateau's law. Therefore, the static force between the foam films is balanced. The balance of force is lost if the stress is above its yield point, and the foam bubbles start sliding along each other in the flow direction. This type of flow is generally characterized by using the three-parameter Herschel-Bulkley model. Another method involves shearing the foam under oscillatory deformation. By analyzing G' and G'' as a function of γ_0 (*i.e.*, amplitude sweep experiment), the large amplitude oscillatory shear (LAOS) behavior is divided into four categories, *i.e.*, shear-thinning, strain-hardening, weak strain overshoot, and strong strain overshoot (Hyun *et al.*, 2002). It has been found that two materials having the same type of amplitude sweep graph may show different nonlinear stress waveforms (Ewoldt *et al.*, 2007; Sugimoto *et al.*, 2006).

Fourier transform (FT) rheology is a sensitive method to deal with nonlinear viscoelastic behavior because it can detect very small oscillatory signals that arise during LAOS (Hyun *et al.*, 2011; Hoyle *et al.*, 2014; Rouyer *et al.*, 2008; Wilhelm *et al.*, 1998; Wilhelm, 2002). Investigating foams by the FT-rheology is challenging because its constituents (*i.e.*, water and air) are Newtonian fluids and have low viscosity. Therefore, amplitude oscillatory tests alone may not be adequate in describing the response under LAOS by means of FT-rheology. Rouyer *et al.* (2008) studied the LAOS behavior of aqueous foams in the full-stress harmonic spectrum to characterize the transition from linear to nonlinear viscoelastic behavior. Ewoldt *et al.* (2008) and Khandavalli and Rothstein (2015) studied the nonlinear viscoelastic properties by analyzing the stress response and the Lissajous-Bowditch curves. These curves are helpful in distinguishing the behavior of

*Corresponding author; E-mail: badri@iitg.ernet.in

foams under deformation. For instance, in a stress vs. strain curve, an ellipsoidal shape characterizes viscous dissipation, while a parallelogram indicates plastic dissipation. Hyun *et al.* (2011) have reviewed the LAOS behavior in detail. Recently, the study of LAOS behavior of food foams stabilized by proteins has been studied (Ptaszek, 2015). Several authors (D'Avino *et al.*, 2013; Gurnon and Wagner, 2012; Jacob *et al.*, 2014; Khair, 2016; Phan-Thien *et al.*, 2000; Rogers and Lettinga, 2012; Wapperom *et al.*, 2005) have developed nonlinear models based on the Giesekus constitutive equation (Giesekus, 1982) and determined nonlinear parameters (Calin *et al.*, 2010; Thompson *et al.*, 2015) to deal with LAOS. Rogers *et al.* (2011a) have proposed an approach, known as a sequence of physical processes, in an intracycle Lissajous-Bowditch curve to a yield stress fluid. The same approach was further used in many more LAOS studies (Kim *et al.*, 2014; Radhakrishnan and Fielding, 2018; Rogers, 2017; Stickel *et al.*, 2013). A great deal of research has been conducted on the linear viscoelastic behavior of foams stabilized by nanoparticles and surfactants (Blanco *et al.*, 2013; Marze *et al.*, 2009; Vishal and Ghosh, 2018), but its nonlinear behavior (*i.e.* LAOS) has hardly been reported. Neither the complex shear dynamic modulus nor the steady flow analysis at the high shear rates have been able to provide physically-meaningful information about the foams.

In this work, we have systematically studied the nonlinear viscoelastic behavior of foam, which was stabilized by a mixture of 0.1 mol m^{-3} hexadecyltrymethylammonium bromide (HTAB) and 0.5% (by weight) silica nanoparticles. The LAOS behavior of foam was described by the stress-response waveforms and Lissajous-Bowditch plots, obtained by shearing the foam at different amplitudes of oscillation. The contributions of higher harmonic oscillatory terms were found by using FT-rheology and the Chebyshev polynomials. Finally, the interpretation of the LAOS behavior of foam was described based on a sequence of physical processes.

2. Theoretical Background

In dynamic oscillatory shear rheology, a material is allowed to flow by imposing a sinusoidal strain in a strain-controlled rheometer. The strain is given by

$$\gamma(\omega,t) = \gamma_0 \sin(\omega t) \tag{1}$$

and the corresponding strain rate is given by

$$\dot{\gamma}(\omega,t) = \omega\gamma_0 \cos(\omega t) \tag{2}$$

where γ_0 and ω are strain amplitude and frequency of oscillation, respectively. When the γ_0 is in the linear viscoelastic regime, the stress response is also sinusoidal with the same ω. It is given by

$$\sigma(\omega,t) = \sigma_0 \sin(\omega t + \delta) \tag{3}$$

where σ_0 is the stress amplitude and δ is the phase angle between the stress response and the imposed strain. Eq. (3) can be decomposed into two parts corresponding to the in- and out-of-phase to strain inputs as follows.

$$\sigma(\omega,t) = \sigma_0 \cos(\delta)\sin(\omega t) + \sigma_0 \sin(\delta)\cos(\omega t) \tag{4a}$$

$$\sigma(\omega,t) = \sigma' \sin(\omega t) + \sigma'' \cos(\omega t) \tag{4b}$$

where σ' and σ'' are the components of the stress response for in- and out-of-phase, respectively.

Two well-defined material functions (*i.e.*, $G' = \sigma'/\gamma_0$ and $G'' = \sigma''/\gamma_0$) are used to characterize the linear viscoelastic behavior of a material. G' describes the elastic behavior and G'' describes the viscous behavior of materials. Eq. (4b) can be written as Macosko (1994)

$$\sigma(\omega,t) = \gamma_0 \left[G'(\omega)\sin(\omega t) + G''(\omega)\cos(\omega t)\right]. \tag{5}$$

In a typical amplitude sweep measurement, both these moduli remain constant up to a certain limiting value of γ_0. The measurement of viscoelastic behavior below and above this limit are termed *linear* and *nonlinear viscoelastic regime*, respectively. In the linear regime, only the first harmonic oscillation is considered for the viscoelastic properties of the materials. However, when a material is deformed in the nonlinear regime, the contribution of higher harmonic terms also becomes significant. Therefore, higher harmonic terms are incorporated into the total stress. Unlike small amplitude oscillatory shear, decomposition of resulting stress into the elastic and viscous components is not very clear under LAOS. Cho *et al.* (2005) suggested a method of decomposing the stress response under LAOS. Their method is based on the symmetrical geometry of the Lissajous-Bowditch curves. It was further improved by Yu *et al.* (2009). It can be expressed by a Fourier series (Wilhelm *et al.*, 1998), given by

$$\sigma(\gamma_0,\omega,t) = \sum_{n=1,3,\cdots} \left[a_n \cos(\omega_n t) + b_n \sin(\omega_n t)\right] \tag{6}$$

where $\omega_n (= 2\pi n)$ is the angular frequency, and a_n and b_n are the Fourier coefficients of the n^{th} harmonic, which relate the applied strain deformation to the stress response as,

$$a_n = \frac{2}{T}\int_0^T \sigma(t)\cos(2\pi n t)dt$$
$$b_n = \frac{2}{T}\int_0^T \sigma(t)\sin(2\pi n t)dt \tag{7}$$

Eq. (6) suggests that only the odd harmonics are included in describing the stress response. Therefore, the nonlinear contributions are captured in the higher-order odd harmonics. This occurs because the resulting stress has odd symmetry with respect to the directionality of shear strain or strain rate (Bird *et al.*, 1987). FT-rheology is a powerful

tool for studying the nonlinear viscoelastic properties of the materials because it can detect even a small signal of higher harmonics. The main advantage of using FT-rheology is that the stress response in LAOS can be expressed as a linear combination of σ' and σ''. It is a linear algebraic analysis method in which σ' and σ'' can be expressed as the orthogonal set of sines and cosines of different frequencies. For the first harmonic (*i.e.*, $n = 1$), Eq. (6) reduces to the linear viscoelastic regime [*i.e.*, Eq. (5)] with $a_1 = \gamma_0 G''$ and $b_1 = \gamma_0 G'$. The intensity of the n^{th} harmonic is defined as

$$I_n = \sqrt{a_n^2 + b_n^2}\,. \tag{8}$$

In addition to I_n, the relative intensity with respect to the first harmonic is an important parameter that provides useful information about the contribution of the higher harmonics in the nonlinear regime. It is defined as

$$I_{n/1} = \sqrt{\frac{a_n^2 + b_n^2}{a_1^2 + b_1^2}}\,. \tag{9}$$

When foam is deformed at sufficiently high amplitudes, higher harmonic terms are observed. This makes the system complex. To avoid such complexity, the time-domain stress-response is converted into frequency-domain by using the FT method. The discrete FT of stress data can be computed as

$$F_n = \sum_{k=0}^{N-1} \sigma_k \exp(-2\pi i n k / N) \tag{10}$$

where k = 0, 1, 2, …, (N–1), N is the total number of experimental data points of the shear stress response, and i is the imaginary unit. F_n represents a signal of the n^{th} harmonic term in the frequency domain of the stress-response. Since F_n is a complex number, it can be expressed by its amplitude.

FT-rheology is a sensitive approach, which determines the amplitude and phase difference of higher harmonics, and may provide useful insights about the progressive transition from linear to nonlinear viscoelastic responses (Wilhelm *et al.*, 1998). However, this approach is not able to elucidate the clear physical interpretation of all the higher harmonic coefficients except the fundamental harmonic (Poulos *et al.*, 2013). Therefore, to avoid these ambiguities, a cycle-by-cycle measurement of the stress response as a function of shear strain (or strain rate) is preferred. A graphical representation of a closed-loop plot of the stress response $\sigma(\gamma_0, \omega, t)$ vs. $\gamma(t)$ [or $\dot{\gamma}(t)$] is termed as *elastic (or viscous) Lissajous-Bowditch curve*. This representation is more convenient for the qualitative analysis of the viscoelastic behavior under LAOS. The elastic and viscous Lissajous-Bowditch curves can be used for decomposing the total shear stress into their elastic and viscous counterparts, respectively, as shown below (Cho *et al.*, 2005; Yu *et al.*, 2009).

$$\sigma\left(\gamma, \frac{\dot{\gamma}}{\omega}\right) = \frac{\sigma\left(\gamma, \frac{\dot{\gamma}}{\omega}\right) + \sigma\left(\gamma, -\frac{\dot{\gamma}}{\omega}\right)}{2} + \frac{\sigma\left(\gamma, \frac{\dot{\gamma}}{\omega}\right) + \sigma\left(-\gamma, \frac{\dot{\gamma}}{\omega}\right)}{2}. \tag{11}$$

σ' at a fixed γ is given by the average of the stress responses obtained during positive and negative strain rates. Similarly, σ'' at a fixed $\dot{\gamma}$ is obtained by taking the average of the shear stress responses at equal magnitude (but opposite signs) of γ.

Ewoldt *et al.* (2008) used the Chebyshev polynomials of the first kind, T_m, to decompose the total stress response in a cycle into their elastic and viscous components. Chebyshev polynomials are defined as $T_m(x) = \cos m\theta$, where $x = \cos\theta$. The recurrence relation of the Chebyshev polynomials is given by Mason and Handscomb (2002)

$$T_m(x) = 2xT_{m-1}(x) - T_{m-2}(x), \quad m = 2,3,\cdots. \tag{12}$$

This, together with the initial conditions, $T_0(x) = 1$ and $T_1(x) = x$, recursively generates all the polynomials $\{T_m(x)\}$ easily. These polynomials are orthogonal over the interval [–1, 1]. Like the FT-rheology approach, the Chebyshev polynomial approach can be utilized in finding the elastic and viscous components of the stress response, given by

$$\begin{aligned} \sigma' &= \gamma_0 \sum_{m\ \text{odd}} e_m(\omega, \gamma_0) T_m(\gamma) \\ \sigma'' &= \dot{\gamma}_0 \sum_{m\ \text{odd}} v_m(\omega, \gamma_0) T_m\left(\frac{\dot{\gamma}}{\omega}\right), \quad m = 2,3,\cdots. \end{aligned} \tag{13}$$

where e_m and v_m are the elastic and viscous Chebyshev coefficients of order m. Based on these coefficients, the materials can be characterized as intracycle strain-hardening ($e_3 > 1$), strain-softening ($e_3 < 1$), shear-thickening ($v_3 > 1$), and shear-thinning ($v_3 < 1$). The Chebyshev coefficients can be utilized to derive the following geometrically-motivated moduli.

$$G'_M \equiv \left.\frac{d\sigma}{d\gamma}\right|_{\gamma=0} = \frac{1}{\gamma_0} \sum_{n\ \text{odd}} n b_n = e_1 - 3e_3 + \cdots, \tag{14}$$

$$G'_L = \left.\frac{\sigma}{\gamma}\right|_{\gamma=\pm\gamma_0} = \sum_{n\ \text{odd}} b_n (-1)^{(n-1)/2} = e_1 + e_3 + \cdots \tag{15}$$

where G'_M is the minimum-strain amplitude at $\gamma = 0$, and G'_L is the large-strain amplitude at $\gamma = \gamma_0$. For the linear viscoelastic regime, both G'_M and G'_L are equivalent to G'. Therefore, this approach of characterizing materials can be considered as more general. However, like FT-rheology, the Chebyshev approach also has limitations when it includes the contribution of the higher harmonic terms above the third. This limitation arises due to the symmetry assumptions for decomposing the total nonlinear stress response into the superposition of an elastic stress and a viscous stress (Poulos *et al.*, 2013; Renou *et al.*, 2010)

[see Eq. (11)]. Rogers and Lettinga (2012) have shown that the physical interpretation of these approaches may vary from one material to another, although they are valuable approaches mathematically.

To interpret the LAOS behavior of a material by using a Lissajous-Bowditch curve, Rogers *et al.* (2011a) have proposed an approach based on a sequence of physical processes. It includes elastic straining, yielding behavior, and flow behavior. The elastic straining during intracycle shearing can be described by the apparent cage modulus (G_{cage}), which can be defined as the derivative of the stress with respect to strain at zero stress.

$$G_{cage} = \left.\frac{d\sigma}{d\gamma}\right|_{\sigma=0} . \quad (16)$$

It is the instantaneous slope of the elastic Lissajous-Bowditch curve at zero stress.

3. Materials and Methods

The cationic surfactant, HTAB, was purchased from Merck (Germany, 97% assay). Negatively-charged silicon dioxide nanoparticles were purchased from Plasmachem (Germany, 92.7% assay). The mean diameter of these particles was ~185 nm. All samples were prepared using water, purified by a Millipore system (France, model: Elix plus Milli-Q). Its resistivity and surface tension were 18.2 MΩ cm and 72.5 mN m^{-1}, respectively.

An aqueous dispersion containing 0.1 mol m^{-3} HTAB and 0.5% (by weight) silica nanoparticles was prepared by mixing the materials using a magnetic stirrer (Tarsons, India, model: MC 02). Higher concentrations of HTAB were not taken because the foams were less stable in the presence of the nanoparticles when the concentration of HTAB was above its critical micelle concentration (CMC) (Vishal and Ghosh, 2018). The aqueous dispersion (200 cm^3) was poured into the jar of a blender (Morphy Richards, India, model: Divo Essentials), and the dispersion was mixed at a speed of 15000 rpm for 30 s. The foam prepared in this manner was used for the rheological studies. Rheological behavior of the foam was studied by using a rotational rheometer (Anton Paar, Germany, model: Physica MCR 301) with a parallel-plate geometry (diameter of plate = 25 mm). Both the plates were roughened by sand blasting to avoid any slip during the experiments. Despite the heterogeneous deformation, the parallel-plate geometry was selected because the gap between the plates could be adjusted easily. The foam was placed between the two plates, and the gap between the plates was fixed at 1 mm during the measurements. The upper plate was moved with the motor connected to the rheometer, and the lower plate remained stationary. The temperature was set to 298 K, and it was controlled within ± 0.1 K using a standard Peltier device. The sensitivity of the rheometer of detecting torque in the rotational mode was 0.1 μNm, and the same for the oscillation mode was 0.02 μNm. The torque resolution was 0.001 μNm. To ensure a perfect sinusoidal strain input, the rheological measurements were carried out by using an electronically-commutated motor in a direct strain oscillation mode (Läuger *et al.*, 2002). To understand the LAOS behavior of foam, we performed the stress analyses at four oscillation frequencies (ω), *i.e.*, 0.1, 1, 10, and 15 rad s^{-1}, and nine strain amplitudes (γ_0), *i.e.*, 1, 6.31, 10, 15.9, 25.1, 39.8, 63.1, 100, and 159%. For each ω and γ_0, the stress was measured as a function of input oscillatory strain (or strain rate) in a complete cycle to produce the Lissajous-Bowditch curves. These curves can be shown in a three-dimensional coordinate system, where strain, strain rate, and stress are the orthogonal coordinate axes. The projections of this curve onto the stress vs. strain and stress vs. strain-rate planes are known as *elastic and viscous Lissajous-Bowditch curve*, respectively (Ewoldt and McKinley, 2010). Each measurement was repeated three times to verify the repeatability. The slip condition was checked by measuring the shear stress as a function of shear rate at different gaps between the parallel plates (Fig. S1 in the supporting information) (Graham, 1995; Habibi *et al.*, 2016; Mooney, 1931). It was observed that the data points almost superposed for all gaps, which confirmed the absence of slip. We have also compared our experimental results with the oscillatory stress response derived for the cone-and-plate geometry (Giacomin *et al.*, 2015), where homogeneous deformation can be achieved (Fig. S2 in the supporting information).

A Fourier series was used to fit the non-sinusoidal stress response obtained from the LAOS experiment. From the stress data points, Fourier coefficients were computed. These coefficients are the in- and out-of-phase stress components of the shear deformation. The relative intensity of the third and the fifth harmonics was determined with respect to the first harmonic term. To study the contribution of the higher harmonic terms to LAOS, the time domain of Fourier series was converted into the frequency domain. Additionally, Chebyshev polynomials were used to fit the Lissajous-Bowditch curves obtained under LAOS.

4. Results and Discussion

Before probing the nonlinear viscoelastic behavior of foam, we performed a few other fundamental experiments on foam as shown in Fig. 1. The results from a typical amplitude sweep experiment on foam are shown in Fig. 1a. This experiment can be used for determining the linear and nonlinear viscoelastic regimes under oscillatory shear. At low strain up to 1%, both G' and G'' were independent of γ_0. This is known as the *linear viscoelastic regime*. Upon increasing γ_0 further (*i.e.* above critical strain ampli-

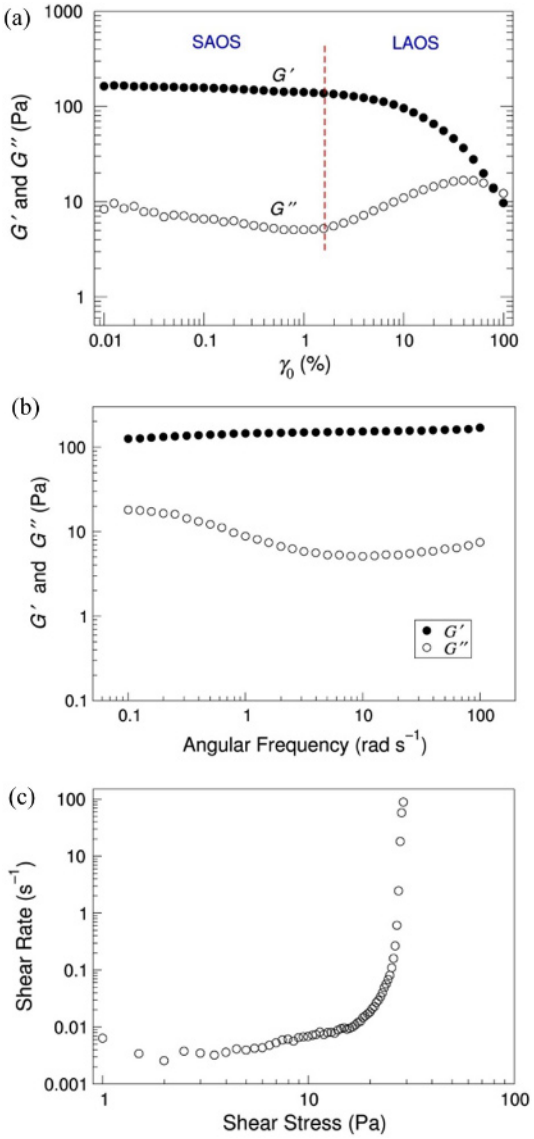

Fig. 1. (Color online) (a) Results from a typical amplitude sweep experiment at $\omega = 1$ rad s^{-1}. (b) Frequency sweep experiment on foam at the constant strain amplitude of 0.5%. (c) Steady state flow curve of the foam.

tude), the foam started yielding. G' decreased continuously, indicating *strain-softening*. G'' initially increased, reached a local maximum at a certain value of γ_0, and then started decreasing. This characteristic is known as *weak strain overshoot*. The overshoot (*i.e.* the local maximum of G'') may be considered as the balance between the formation and destruction of the structure of foams (Hyun *et al.*, 2002). The yield strain is usually considered at the crossover point of G' and G'' (Moller *et al.*, 2009). As the strain amplitude exceeded the yield point, both the moduli decreased (with $G'' > G'$) indicating the liquid-like behavior. Therefore, yielding can be considered as the transition of a material from solid-like to liquid-like behavior. The response of foam after 1% γ_0 is known as the *nonlinear viscoelastic regime*, where the LAOS experiment was performed.

G' and G'' are suitable rheological parameters for explaining the viscoelastic behavior in the linear viscoelastic regime, as they contain only the first harmonic contributions to the stress response. The intensities of other odd higher harmonics in medium amplitude oscillatory shear regions are very small. However, higher harmonic contributions must be added to distinguish and investigate the viscoelastic behavior at large γ_0. The linear viscoelastic moduli of the foam were plotted as a function of frequency in Fig. 1b. These moduli were obtained at the constant strain amplitude of 0.5% because at this amplitude foam exhibited linear viscoelastic behavior (see Fig. 1a). Additionally, G' was one order of magnitude higher than G'', and both the moduli were independent of the fre-

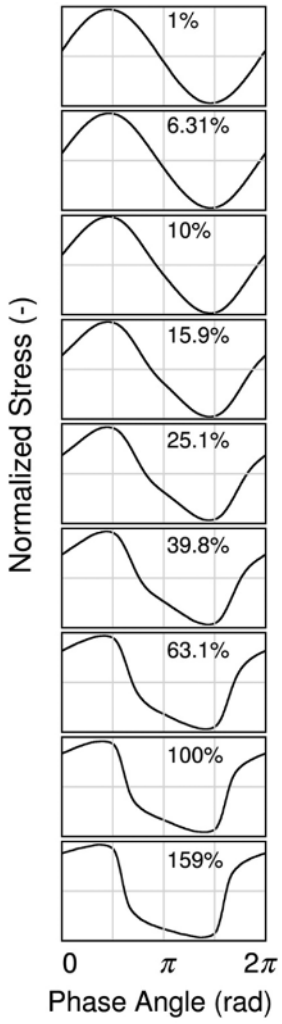

Fig. 2. The waveform of the shear stress as a function of phase angle in a complete cycle. The shear stress results were obtained by imposing oscillatory shear strain at different amplitudes ranging from 1 to 159%.

quency of oscillation, which is a typical gel-like behavior. The steady state flow curve of the foam is shown in Fig. 1c. The shear rate was measured by varying the shear stress. We observed that there was no flow below ~15 Pa shear stress because the shear rate was almost zero, which implies that the foam showed yield stress.

Because of the non-sinusoidal shape of the stress waveform, the complex shear modulus alone is not sufficient to characterize the foam behavior. Therefore, to investigate the nonlinear viscoelastic behavior of the foam, analysis of the stress response waveform can be useful. The waveform depends on the structure of foam. When foam was deformed under LAOS, the stress response was still periodic, and the stress curves changed their shape from sinusoidal to non-sinusoidal with increasing strain amplitude as shown in Fig. 2. The asymmetry of the stress response was significant with increasing γ_0. A shape signifying "backward tilted stress" was observed under LAOS. The third harmonic term is mainly responsible for the non-sinusoidal shape of the waveform. The other higher harmonic terms typically decay rapidly. The effects of higher harmonic terms were also studied by using Fourier series, which are reported later in this section.

The elastic Lissajous-Bowditch curves of foam are shown in Fig. 3. In the linear viscoelastic regime, the Lissajous-Bowditch curves were elliptic. The slope of the major axis of the ellipse represents the magnitude of the complex shear modulus. With increasing γ_0, the width of the minor axis of the ellipse became wider, which can be attributed to the phase angle between input strain and output stress (Erni and Parker, 2012). Additionally, the shape of the Lissajous-Bowditch curves became increasingly rectangular with highly-rounded corners. This can be seen clearly in Fig. 3 for $\gamma_0 > 39.8\%$. This shape implies that the greatest increase in stress occurred when the strain was maximum in a cycle. These increasingly rectangular elastic Lissajous-Bowditch curves confirm the intracycle strain-hardening process associated with the foam under LAOS. In the nonlinear viscoelastic regime, however, the shape of the Lissajous-Bowditch curves was more complex and

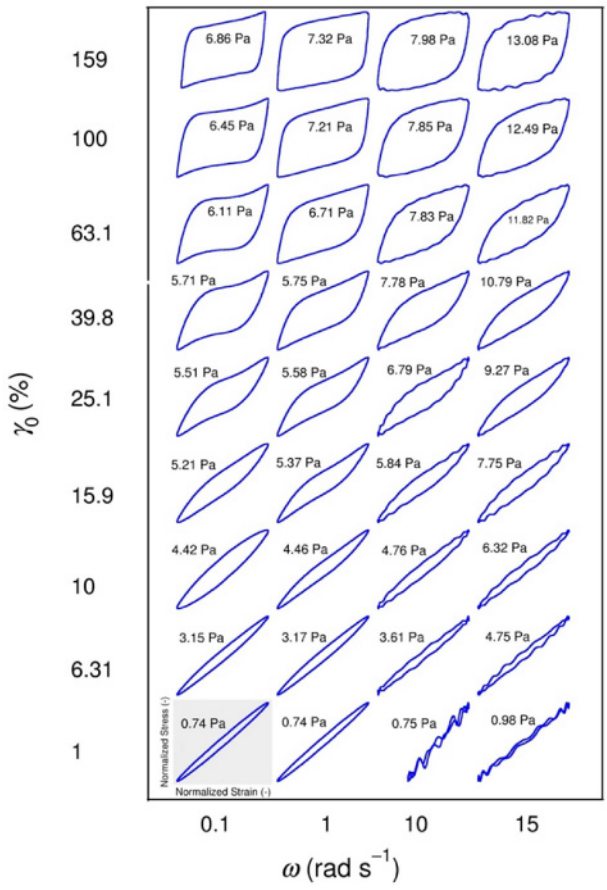

Fig. 3. (Color online) Elastic Lissajous-Bowditch curves [normalized stress, $\sigma(t)/\sigma_0$ vs. normalized strain, $\gamma(t)/\gamma_0$]. The amplitude of shear stress (σ_0) is indicated in each curve. All curves are two-dimensional projections of the three-dimensional curves on the stress-strain plane.

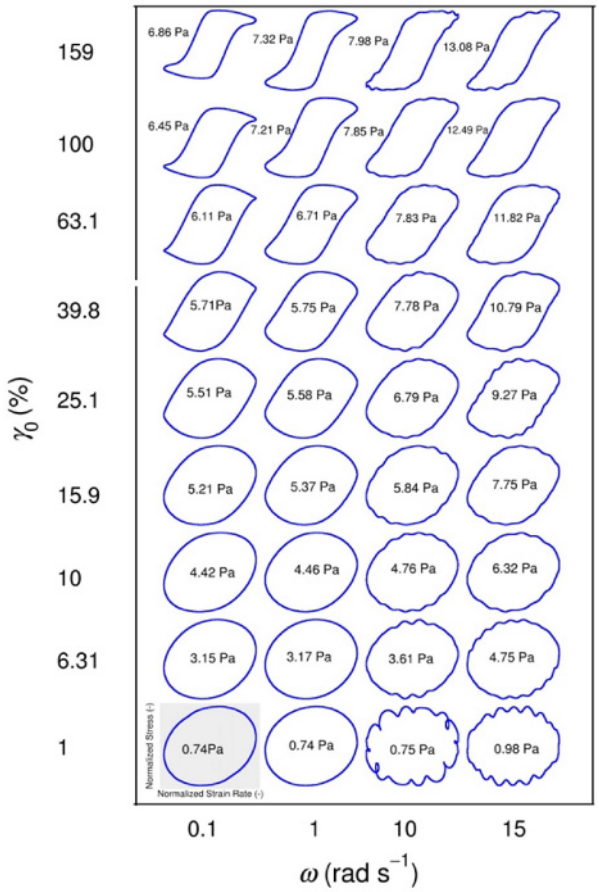

Fig. 4. (Color online) Viscous Lissajous-Bowditch curves [normalized stress, $\sigma(t)/\sigma_0$ vs. normalized strain rate, $\gamma(t)/\gamma_0$]. The amplitude of shear stress (σ_0) is indicated in each curve. All curves are two-dimensional projections of the three-dimensional curves on the stress-strain rate plane.

non-ellipsoidal. Therefore, the simple viscoelastic moduli may not be appropriate to explain the real shape, and they may mislead much of the structural and physical information. The area enclosed by the elastic Lissajous-Bowditch curves increased with γ_0, which indicates an increase in the energy dissipated during the LAOS test.

The data suffered from noise in the right bottom portions in Figs. 3 and 4. This may be due to the fact that at high ω, the experimental time was less than the time required for the foam to relax. The stress amplitude increased with increasing ω. However, the shape of the Lissajous-Bowditch curves remained almost unchanged. A progressive transition from linear to nonlinear behavior can be observed from the elastic Lissajous-Bowditch curves. The onset of nonlinearity of the foam can be visually observed for strain above 10%, as the shape of the Lissajous-Bowditch curve (or stress response waveform) started changing at this point onward. The corresponding viscous Lissajous-Bowditch curves have been shown in Fig. 4. These curves showed sigmoid shape under LAOS, which confirmed the intracycle shear-thinning behavior (López-Barrón *et al.*, 2015). The instantaneous viscosity of the foam can be found from the slope of the viscous Lissajous-Bowditch curves. The instantaneous viscosity decreased with increasing deformation rate. Therefore, the foam showed intracycle shear-thinning behavior. The 3D curves of the Lissajous-Bowditch plots are shown at different projection angles in Fig. S3 in the supporting information.

The elastic component of the total stress showed the linear dependency on strain at low γ_0. The stress-strain curve was bent upward at large strains, as shown in Fig. 5. This shape is often considered as an indication of strain-hardening (Papon *et al.*, 2010). In contrary, the amplitude sweep experiment showed strain-softening of the foam (Fig. 1). This paradox has been reported recently by Mermet-Guyennet *et al.* (2015). They concluded that the

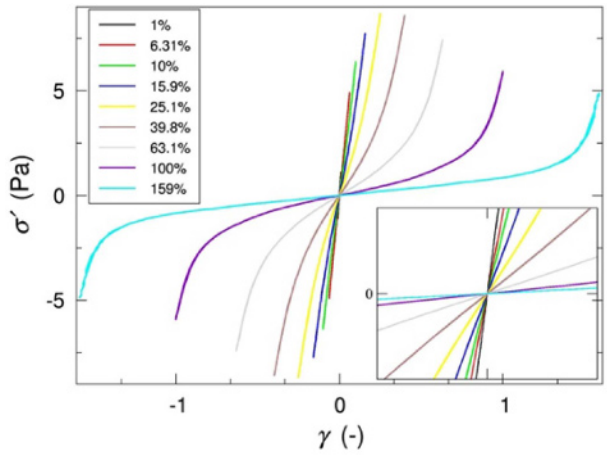

Fig. 5. (Color online) The elastic components of the shear stress response (obtained from Fig. 3) as a function of strain in one period of oscillation. The experiment was performed at $\omega = 1$ rad s^{-1} for different strain amplitudes (γ_0) ranging from 1 to 159%.

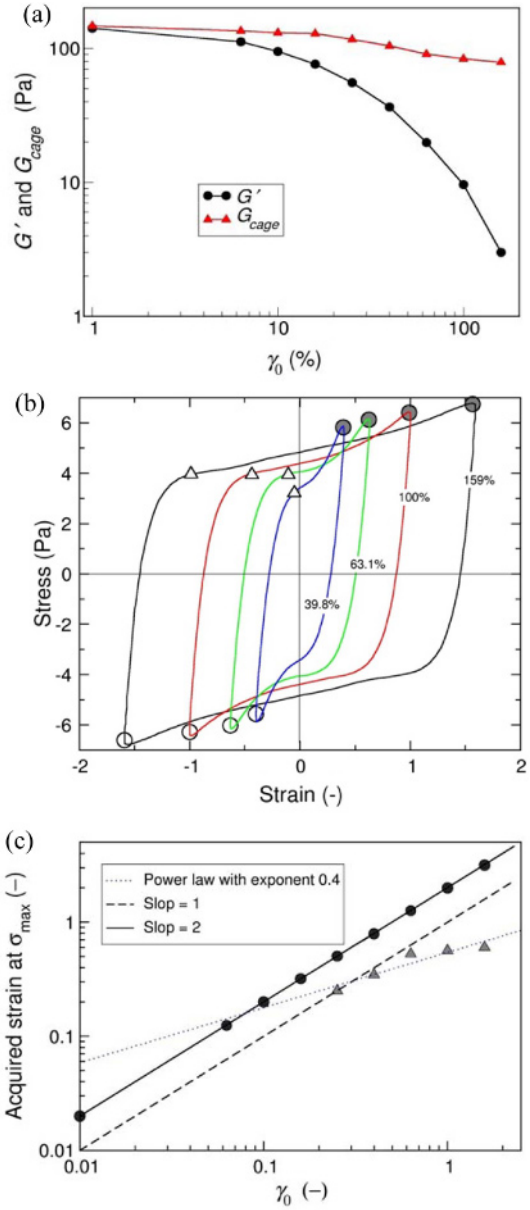

Fig. 6. (Color online) (a) Storage modulus (G') and apparent cage modulus (G_{cage}) as a function of strain amplitude (γ_0). (b) The elastic Lissajous-Bowditch curves of the foam at the selected strain amplitudes under LAOS. The empty circles indicate the lower reversal point, triangles represent maximum elastic points (*i.e.* stress overshoot), and filled circles indicate the point of maximum total stress. (c) The strain required from the lower reversal point to the point of maximum total stress (circles) and maximum elastic stress (triangles) as a function of strain amplitude. Idealized behavior of elastic solid and viscous liquid are represented by solid and dashed lines, respectively. The strain required to reach the maximum elastic point follows power law with index 0.4 (dashed line).

strain-hardening was due to the use of G_M'. However, the overall LAOS behavior indicated strain-softening. To investigate further the nonlinear viscoelastic behavior of foam, we adopted the approach of sequence of physical processes proposed by Rogers *et al.* (2011a). This approach provides a framework to analyze the intracycle response of the elastic Lissajous-Bowditch curves by decomposing it into the sequence of physical processes, *i.e.*, elastic straining, yielding behavior, and flow behavior. Fig. 6a shows the G_{cage} (determined from Eq. (16)) and G' (see Fig. 1a) as a function of γ_0. Both the moduli overlap in the linear viscoelastic regime indicating that the foam extended in a linear fashion. The G' decreased with increasing strain amplitude, but G_{cage} did not change significantly and remained significantly above the G', even at the higher amplitudes. This indicates that the foam exhibited an elastic deformation. It also suggests that the foam behaved according to the sequence of physical processes (Rogers *et al.*, 2011b).

In addition, the elastic straining can be illustrated more clearly from the elastic Lissajous-Bowditch curves as shown in Fig. 6b. At the strain reversion point (*i.e.* maximum strain or zero strain rate), the stress increased almost linearly with strain up to the critical strain, which implies the elastic behavior of foam. Further increasing the strain above the critical point, the stress continued to increase until a yield stress was achieved, where it showed an overshoot (or a local maxima) (see the top left curves of Fig. 3). The yielding behavior can be characterized by determining the total strain required from the lower reversal point (unfilled circles) to the point of maximum elastic stress (triangle) and maximum total stress (filled circles) from Fig 6b. These accumulated strains are shown in Fig. 6c as a function of γ_0. For an ideal elastic solid, the amount of strain required to achieve the maximum total stress is $2\gamma_0$, whereas this value is γ_0 for the ideal viscous liquid. The idealized behavior of elastic solid and viscous liquid is represented by the solid and dashed lines, respectively (see Fig. 6c). The data points corresponding to the maximum total stress followed a straight line with slope 2. This implies that the maximum total stress was caused by an elastic process. Therefore, the foam structure reformed after the strain corresponding to the maximum total stress by releasing the elastic stress. On the other hand, the maximum elastic stress initially followed a straight line with slope 1, indicating that the stress was caused by a viscous process. The data points deviated at large amplitudes, and they followed the power-law behavior with flow index 0.4. This confirms the shear-thinning flow behavior of foam above the yield stress. van der Vaart *et al.* (2013) observed similar kind of results for a concentrated soft-sphere suspension. However, for hard-sphere suspension, the acquired strain to maximum total stress followed perfect solid-like behavior at low γ_0 and perfect liquid-like behavior at high γ_0 (Rogers *et al.*, 2011a; van der Vaart *et al.*, 2013). The flow behavior above the yield strain can be initially characterized as viscoplastic because the stress remained almost constant, and then it increased abruptly with strain indicating strain-hardening behavior. This sequence of physical processes was repeated in the remaining half-cycle of the oscillation.

One aspect of studying the yielding behavior is the appearance of significant non-linearity. From the elastic Lissajous-Bowditch curves under LAOS at higher frequency (see the top right curves of Fig. 3), it appears that the foam exhibited plastic and/or elastoplastic flow beyond the yield strain. To deal with such flow behavior in a cyclic deformation, the concept of kinematic hardening is widely used (Dimitriou and McKinley, 2014; Fraggedakis *et al.*, 2016). This concept describes the stress-strain relationship for yielding materials. Dimitriou *et al.* (2013) have developed a method to understand the kinematic hardening from the Lissajous-Bowditch curves. Their method is based on the elastic Herschel-Bulkley model. In this method, the strain at a point on the elastic Lissajous-Bowditch curve can be decomposed into elastic (γ^e) and plastic (γ^p) components as

$$\gamma = \gamma^e + \gamma^p . \tag{17}$$

The stress is related to γ^e through the Young's modulus (G) as $\sigma = G\gamma^e$, and the elastic strain retain beyond the yield point. The contribution to the stress due to plastic flow is called *back stress* (σ_{back}). The plastic flow rate ($\dot{\gamma}^p$) is related to the effective stress (*i.e.* $|\sigma - \sigma_{back}|$), which is the driving force for the plastic flow. It is given by (Dimitriou *et al.*, 2013),

$$\dot{\gamma}^p = n^p \left[\frac{|\sigma - \sigma_{back}|}{k} \right]^{1/q} \tag{18}$$

where n^p is the direction of plastic flow, and k and q are the consistency index and the flow index, respectively. Below the yield strain, it is assumed that $\dot{\gamma}^p$ is zero, and the foam undergoes only elastic deformation. However, above the yield strain, the rate-independent plastic flow begins to occur. This is immediately followed by strain-hardening at low frequency and kinematic hardening at high frequency. At the strain reversal point, the elastic strain is recovered and the cycle is repeated by dropping the stress below their yield value.

Eqs. (6) and (13) show the relation between the FT-rheology and the Chebyshev polynomial approaches. Both the approaches are based on linear algebraic analysis, where elastic and viscous components of the total stress response can be expressed as a linear combination of the finite orthogonal basis sets. In the FT-rheology approach, σ' and σ'' are expressed as the linear combination of the orthogonal sets of sines and cosines, respectively, of dif-

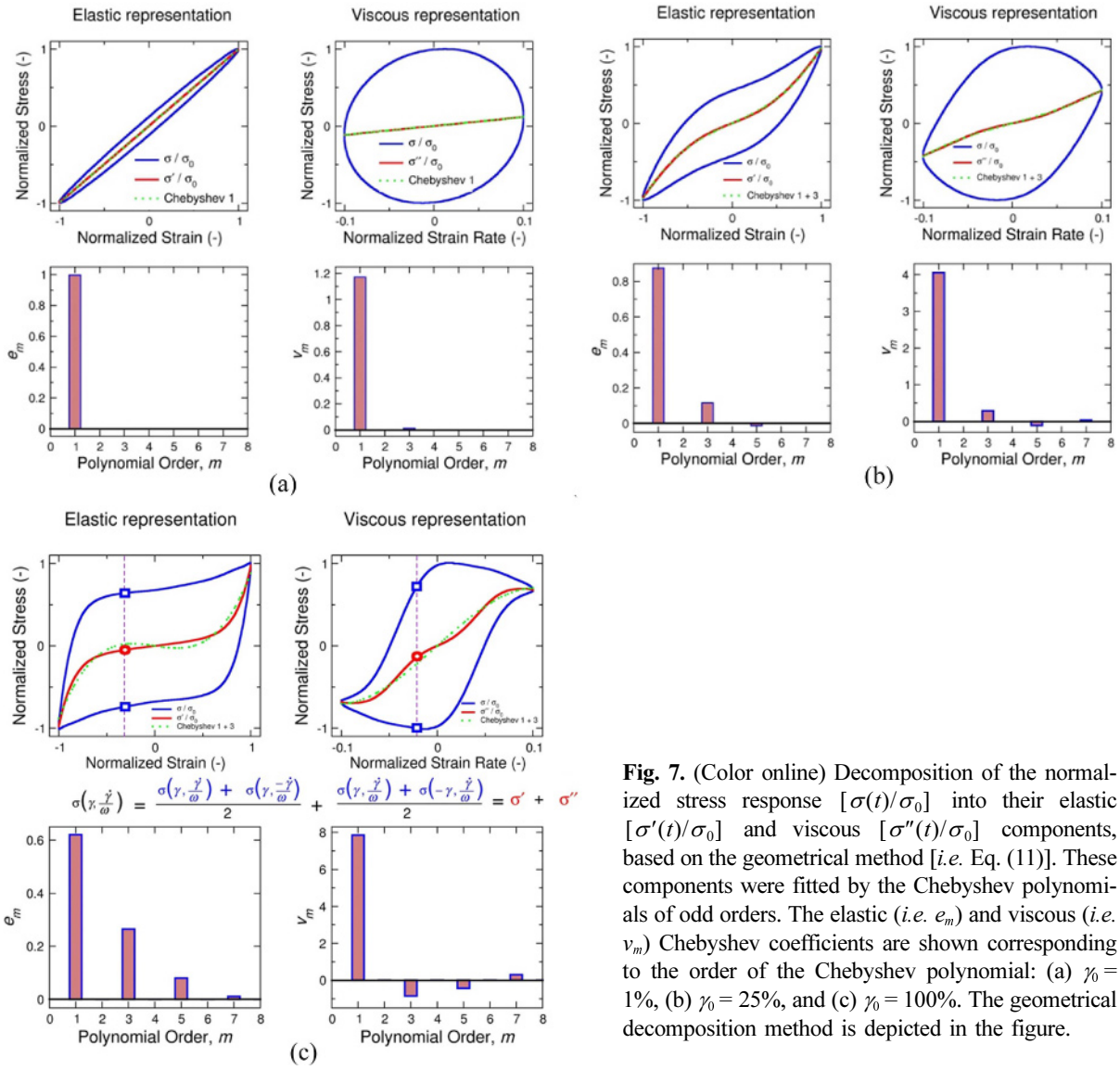

Fig. 7. (Color online) Decomposition of the normalized stress response $[\sigma(t)/\sigma_0]$ into their elastic $[\sigma'(t)/\sigma_0]$ and viscous $[\sigma''(t)/\sigma_0]$ components, based on the geometrical method [*i.e.* Eq. (11)]. These components were fitted by the Chebyshev polynomials of odd orders. The elastic (*i.e.* e_m) and viscous (*i.e.* v_m) Chebyshev coefficients are shown corresponding to the order of the Chebyshev polynomial: (a) γ_0 = 1%, (b) γ_0 = 25%, and (c) γ_0 = 100%. The geometrical decomposition method is depicted in the figure.

ferent higher odd harmonic frequencies. In the Chebyshev polynomial approach, σ' and σ'' are expressed as the linear combination of the orthogonal sets of Chebyshev polynomials of different higher odd orders. The FT-rheology approach is not able to elucidate the physical interpretation of all the higher harmonic coefficients except the fundamental harmonic. However, the Chebyshev approach can be used to interpret the LAOS results within a cycle by using the first and third Chebyshev coefficients. Like the FT approach, the first Chebyshev coefficient explains the linear viscoelastic behavior. The elastic and viscous components of the total shear stress obtained from the corresponding Lissajous-Bowditch curves are shown in Fig. 7. These stress components were obtained by taking the average of the shear stresses during positive and negative $\dot{\gamma}$ (or γ) at a fixed γ (or $\dot{\gamma}$). This method of decomposing the stress response was proposed by Cho *et al.* (2005), and it is useful for analyzing the viscoelastic properties of foam under LAOS. Furthermore, these stress components were fitted by Chebyshev polynomials. As can be seen from Fig. 7a, when foam was deformed in the linear viscoelastic regime (*i.e.* at 1% γ_0), σ' increased linearly with γ, and σ'' was almost independent of $\dot{\gamma}$. This implies that the foam showed a predominantly elastic behavior. Also, due to the linear viscoelastic properties, the first-degree Chebyshev polynomial was alone sufficient to fit the stress components. The linearity can also be confirmed from the Chebyshev coefficients, inasmuch as both e_3 and v_3 were zero. Upon further increasing γ_0 to 25%, it was found that the σ' and σ'' components were not linearly dependent on γ and $\dot{\gamma}$, respectively. Therefore, third-order Chebyshev polynomials were used to fit the stress components. Both e_3 and v_3 were positive, which implies that the foam showed strain-hardening and shear-thicken-

ing behavior. At very high γ_0 (*e.g.* 100%), a sudden rise in σ' was observed at large γ, which reflects that the foam was stiff. A positive value of e_3 confirms the intracycle strain-hardening behavior. In contrast, the slope of the σ'' vs. $\dot{\gamma}$ curve decreased, and v_3 was negative. Therefore, the foam showed an intracycle shear-thinning behavior.

Fig. S4 in the supporting information clearly shows the contribution of the higher harmonic terms under the LAOS response. The solid line shows the experimental stress response, and the dashed line depicts the stress obtained from the Fourier series [*i.e.*, Eq. (6)]. The Fourier coefficients (*i.e.*, a_n and b_n) were computed from Eq. (7). These are shown in the corresponding figures. When foam was deformed at low γ_0 (up to ~6.31%), only the first harmonic term was sufficient to fit the stress response waveforms. With increasing γ_0, higher odd harmonic terms were required. Therefore, the third harmonic term, along with the first term, fitted the stress waveform (up to 25.1%). Further increasing γ_0, the fifth-term was required, and it was added to fit the stress response waveforms. It was observed that the even terms did not make any contribution to LAOS. It reconfirmed the absence of the slip condition between the two parallel plates, where the foam was placed. Each peak in Fig. S1 in the supporting information in the first column represents the magnitude of the corresponding harmonic terms. This is known as the *FT-rheology spectrum*. These peaks were determined by discrete FT of stress data using Eq. (10). From the figure, it is clearly seen that the number of higher harmonic contributions and the magnitude of the peaks at odd harmonics increased with applied γ_0.

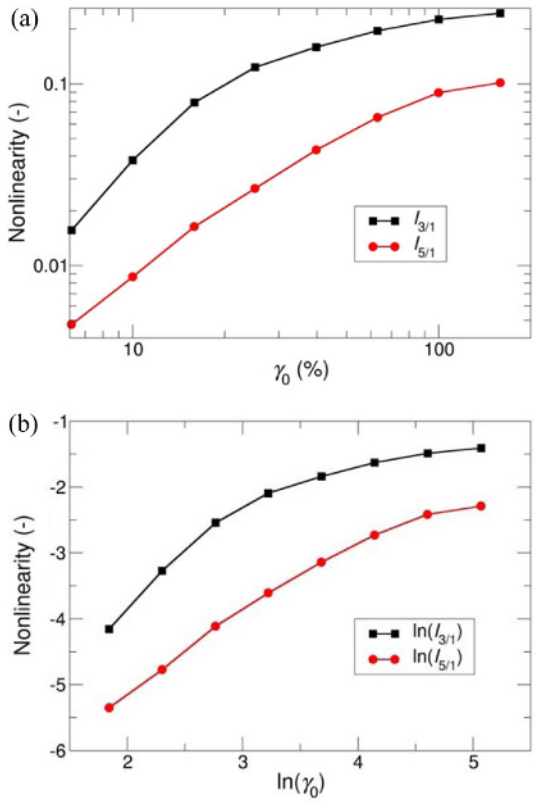

Fig. 8. (Color online) (a) Relative intensity of the third harmonic ($I_{3/1}$) and fifth harmonic ($I_{5/1}$) expressed as a function of the shear strain amplitude (γ_0) (*i.e.*, Eq. (9)). (b) Relative intensity ($I_{3/1}$ and $I_{5/1}$) computed by taking logarithm of the data in Fig. 8a. The experiment was performed by applying an oscillatory shear at $\omega = 1$ rad s^{-1}.

The nonlinearity was quantified by determining the relative intensities of higher harmonic terms with respect to the first (*i.e.*, fundamental) harmonic (*e.g.*, $I_{3/1}$ and $I_{5/1}$), as shown in Fig. 8. $I_{3/1}$ increased linearly with increasing γ_0 (up to ~25%). With further increase in γ_0, $I_{3/1}$ increased slowly. This may be due to the presence of the third harmonic term. $I_{3/1}$ increased linearly up to 100% γ_0. The contribution of the higher harmonic terms became significant when the foam was deformed at high γ_0. When ln($I_{3/1}$) was plotted against ln(γ_0), a straight line with slope ~2 was obtained in the low-to-medium γ_0 range, as shown in Fig. 8b. This indicates a scaling relationship between $I_{3/1}$ and γ_0 (Hyun and Wilhelm, 2008; Wagner *et al.*, 2011). At low-to-medium shear deformation, $I_{3/1}$ of the foam varied quadratically with γ_0. A similar result was observed for beer foams (Wilhelm *et al.*, 2012). The third harmonic is the best corresponding to the scaling theory at the small amplitude. An asymptotic behavior to a plateau value was observed at high γ_0. Therefore, the scaling theory was not suitable for the relative intensity higher than the third harmonic. However, an attempt was made to extend the scaling law for $I_{5/1}$. It was found that it varied linearly over a wide range of γ_0, as shown in Fig. 8.

5. Conclusions

Nonlinear viscoelastic behavior of foam stabilized by HTAB and silica nanoparticles was systematically studied under LAOS by using Lissajous-Bowditch curves, FT-rheology analysis, and the Chebyshev polynomial technique. The LAOS results were interpreted based on the sequence of physical processes. With increasing γ_0, the shape of the waveforms and the Lissajous-Bowditch curves changed. Elastic Lissajous-Bowditch curves changed from ellipsoidal to rectangular, which shows the strain-hardening behavior of foam. However, the overall behavior was shear-thinning. Flow under LAOS was periodic, and it involved the contributions of the higher odd harmonic terms to the stress response. The peaks corresponding to the even harmonic oscillatory terms were not observed, which may be due to the "no slip" condition between the parallel plates, where the foam was placed during the LAOS test. The foam showed linear elastic response in the linear viscoelastic regime as e_3 was zero. Intracycle strain-hardening behavior was observed in the nonlinear visco-

elastic regime as e_3 was positive. Furthermore, it showed linear viscous response in the linear viscoelastic regime (as v_3 was zero), intracycle shear-thickening at moderate γ_0 (as v_3 was positive), and intracycle shear-thinning at high γ_0 (as v_3 was negative). It was also observed that $I_{3/1}$ was quadratically dependent on γ_0 at low-to-intermediate shear deformation. However, $I_{5/1}$ varied linearly over a wide range of γ_0. G_L' was greater than G_M' in the entire range of amplitude and frequency of oscillation under LAOS, which also confirmed the strain-hardening behavior of foam. The sequence of physical processes revealed that the foam exhibited elastic straining at the strain reversion point and showed yielding above the critical strain, which was followed by strain-hardening. It also showed kinematic hardening at high frequency under LAOS flow.

List of Symbols

a_n : Fourier cosine coefficient of the n^{th} harmonic [Pa]
b_n : Fourier sine coefficient of the n^{th} harmonic [Pa]
e_m : Elastic Chebyshev coefficient of order m [-]
F_n : Discrete FT of the n^{th} harmonic [-]
G : Young's modulus [-]
G' : Storage modulus [Pa]
G'' : Loss modulus [Pa]
G_{cage} : Cage modulus [Pa]
G_L' : Large-strain amplitude [Pa]
G_M' : Minimum-strain amplitude [Pa]
I_n : Intensity of n^{th} harmonic [Pa]
$I_{n/1}$: Relative intensity of n^{th} harmonic [-]
i : Imaginary unit [-]
k : Consistency index [-]
m : Order of Chebyshev polynomial of the first kind [-]
N : Total number of data points [-]
n : Harmonic [-]
n^p : Direction of plastic flow [-]
q : Flow index [-]
T : Time period [s]
T_m : Chebyshev polynomial of the first kind [-]
t : Time [s]
v_m : Viscous Chebyshev coefficient of order m [-]

Greek Symbols

γ : Shear strain [-]
$\dot{\gamma}$: Strain rate [s^{-1}]
$\dot{\gamma}^p$: Plastic flow rate [s^{-1}]
γ_0 : Strain amplitude [-]
γ^e : Elastic strain [-]
γ^p : Plastic strain [-]
δ : Phase angle [rad]
σ : Shear stress [Pa]
σ' : In-phase shear stress component [Pa]
σ'' : Out-of-phase shear stress component [Pa]
σ_{back} : Back stress [Pa]
σ_0 : Stress amplitude [Pa]
ω : Angular frequency [rad s^{-1}]

Abbreviations

CMC : Critical micelle concentration
FT : Fourier transform
HTAB : Hexadecyltrymethylammonium bromide
LAOS : Large amplitude oscillatory shear

References

Ahmadi, Y., S.E. Eshraghi, P. Bahrami, M. Hasanbeygi, Y. Kazemzadeh, and A. Vahedian, 2015, Comprehensive water-alternating-gas (WAG) injection study to evaluate the most effective method based on heavy oil recovery and asphaltene precipitation tests, *J. Pet. Sci. Eng.* **133**, 123-129.

Balmforth, N.J., I.A. Frigaard, and G. Ovarlez, 2014, Yielding to stress: Recent developments in viscoplastic fluid mechanics, *Annu. Rev. Fluid Mech.* **46**, 121-146.

Bird, R.B., R.C. Armstrong, and O. Hassager, 1987, *Dynamics of Polymeric Liquids, Volume 1: Fluid Mechanics* John Wiley & Sons, New York.

Blanco, E., S. Lam, S.K. Smoukov, K.P. Velikov, S.A. Khan, and O.D. Velev, 2013, Stability and viscoelasticity of magneto-pickering foams, *Langmuir* **29**, 10019-10027.

Calin, A., M. Wilhelm, and C. Balan, 2010, Determination of the non-linear parameter (mobility factor) of the Giesekus constitutive model using LAOS procedure, *J. Non-Newton. Fluid Mech.* **165**, 1564-1577.

Cho, K.S., K. Hyun, K.H. Ahn, and S.J. Lee, 2005, A geometrical interpretation of large amplitude oscillatory shear response, *J. Rheol.* **49**, 747-758.

D'Avino, G., F. Greco, M.A. Hulsen, and P.L. Maffettone, 2013, Rheology of viscoelastic suspensions of spheres under small and large amplitude oscillatory shear by numerical simulations, *J. Rheol.* **57**, 813-839.

Denkov, N.D., S. Tcholakova, K. Golemanov, K.P. Ananthapadmanabhan, and A. Lips, 2008, Viscous friction in foams and concentrated emulsions under steady shear, *Phys. Rev. Lett.* **100**, 138301.

Denkov, N.D., S. Tcholakova, K. Golemanov, K.P. Ananthpadmanabhan, and A. Lips, 2009, The role of surfactant type and bubble surface mobility in foam rheology, *Soft Matter* **5**, 3389-3408.

Dickinson, E., 2015, Structuring of colloidal particles at interfaces and the relationship to food emulsion and foam stability, *J. Colloid Interface Sci.* **449**, 38-45.

Dimitriou, C.J. and G.H. McKinley, 2014, A comprehensive constitutive law for waxy crude oil: A thixotropic yield stress fluid, *Soft Matter* **10**, 6619-6644.

Dimitriou, C.J., R.H. Ewoldt, and G.H. McKinley, 2013, Describing and prescribing the constitutive response of yield stress flu-

ids using large amplitude oscillatory shear stress (LAOStress), *J. Rheol.* **57**, 27-70.

Erni, P. and A. Parker, 2012, Nonlinear viscoelasticity and shear localization at complex fluid interfaces, *Langmuir* **28**, 7757-7767.

Ewoldt, R.H., A.E. Hosoi, and G.H. McKinley, 2008, New measures for characterizing nonlinear viscoelasticity in large amplitude oscillatory shear, *J. Rheol.* **52**, 1427-1458.

Ewoldt, R.H., C. Clasen, A.E. Hosoi, and G.H. McKinley, 2007, Rheological fingerprinting of gastropod pedal mucus and synthetic complex fluids for biomimicking adhesive locomotion, *Soft Matter* **3**, 634-643.

Ewoldt, R.H. and G.H. McKinley, 2010, On secondary loops in LAOS via self-intersection of Lissajous-Bowditch curves, *Rheol. Acta* **49**, 213-219.

Fraggedakis, D., Y. Dimakopoulos, and J. Tsamopoulos, 2016, Yielding the yield-stress analysis: a study focused on the effects of elasticity on the settling of a single spherical particle in simple yield-stress fluids, *Soft Matter* **12**, 5378-5401.

Giacomin, A.J., P.H. Gilbert, D. Merger, and M. Wilhelm, 2015, Large-amplitude oscillatory shear: Comparing parallel-disk with cone-plate flow, *Rheol. Acta* **54**, 263-285.

Giesekus, H., 1982, A simple contitutive equation for polymer fluids based on the concept of deformation-dependent tensorial mobility, *J. Non-Newton. Fluid Mech.* **11**, 69-109.

Graham, M.D., 1995, Wall slip and the nonlinear dynamics of large amplitude oscillatory shear flows, *J. Rheol.* **39**, 697-712.

Gurnon, A.K. and N.J. Wagner, 2012, Large amplitude oscillatory shear (LAOS) measurements to obtain constitutive equation model parameters: Giesekus model of banding and nonbanding wormlike micelles, *J. Rheol.* **56**, 333-351.

Habibi, M., M. Dinkgreve, J. Paredes, M.M. Denn, and D. Bonn, 2016, Normal stress measurement in foams and emulsions in the presence of slip, *J. Non-Newton. Fluid Mech.* **238**, 33-43.

Höhler, R. and S. Cohen-Addad, 2005, Rheology of liquid foam, *J. Phys.:Condens. Matter* **17**, 1041-1069.

Hoyle, D.M., D. Auhl, O.G. Harlen, V.C. Barroso, M. Wilhelm, and T.C.B. McLeish, 2014, Large amplitude oscillatory shear and Fourier transform rheology analysis of branched polymer melts, *J. Rheol.* **58**, 969-997.

Hyun, K. and M. Wilhelm, 2008, Establishing a new mechanical nonlinear coefficient Q from FT-rheology: First investigation of entangled linear and comb polymer model systems, *Macromolecules* **42**, 411-422.

Hyun, K., M. Wilhelm, C.O. Klein, K.S. Cho, J.G. Nam, K.H. Ahn, S.J. Lee, R.H. Ewoldt, and G.H. McKinley, 2011, A review of nonlinear oscillatory shear tests: Analysis and application of large amplitude oscillatory shear (LAOS), *Prog. Polym. Sci.* **36**, 1697-1753.

Hyun, K., S.H. Kim, K.H. Ahn, and S.J. Lee, 2002, Large amplitude oscillatory shear as a way to classify the complex fluids, *J. Non-Newton. Fluid Mech.* **107**, 51-65.

Jacob, A.R., A.P. Deshpande, and L. Bouteiller, 2014, Large amplitude oscillatory shear of supramolecular materials, *J. Non-Newton. Fluid Mech.* **206**, 40-56.

Khair, A.S., 2016, Large amplitude oscillatory shear of the Giesekus model, *J. Rheol.* **60**, 257-266.

Khan, S.A. and R.C. Armstrong, 1986, Rheology of foams: 1. Theory for fry foams, *J. Non-Newton. Fluid Mech.* **22**, 1-22.

Khandavalli, S. and J.P. Rothstein, 2015, Large amplitude oscillatory shear rheology of three different shear-thickening particle dispersions, *Rheol. Acta* **54**, 601-618.

Kim, J., D. Merger, M. Wilhelm, and M.E. Helgeson, 2014, Microstructure and nonlinear signatures of yielding in a heterogenous colloidal gel under large amplitude oscillatory shear, *J. Rheol.* **58**, 1359-1390.

Labiausse, V., R. Höhler, and S. Cohen-Addad, 2007, Shear induced normal stress differences in aqueous foams, *J. Rheol.* **51**, 479-492.

Läuger, J., K. Wollny, and S. Huck, 2002, Direct strain oscillation: A new oscillatory method enabling measurements at very small shear stresses and strains, *Rheol. Acta* **41**, 356-361.

López-Barrón, C.R., N.J. Wagner, and L. Porcar, 2015, Layering, melting, and recrystallization of a close-packed micellar crystal under steady and large amplitude oscillatory shear flows, *J. Rheol.* **59**, 793-820.

Macosko, C.W., 1994, *Rheology: Principles, Measurements, and Applications*, Wiley-VCH, New York.

Marze, S., R.M. Guillermic, and A. Saint-Jalmes, 2009, Oscillatory rheology of aqueous foams: Surfactant, liquid fraction, experimental protocol and aging effects, *Soft Matter* **5**, 1937-1946.

Mason, J.C. and D.C. Handscomb, 2002, *Chebyshev Polynomials*, Chapman and Hall/CRC, Boca Raton.

Mermet-Guyennet, M.R.B., J. Gianfelice de Castro, M. Habibi, N. Martzel, M.M. Denn, and D. Bonn, 2015, LAOS: The strain softening/strain hardening paradox, *J. Rheol.* **59**, 21-32.

Moller, P., A. Fall, V. Chikkadi, D. Derks, and D. Bonn, 2009, An attempt to categorize yield stress fluid behaviour, *Philos. Trans. R. Soc. Lond Ser. A-Math. Phys. Eng. Sci.* **367**, 5139-5155.

Mooney, M., 1931, Explicit formulas for slip and fluidity, *J. Rheol.* **210**, 210-222.

Papon, A., H. Montes, F. Lequeux, and L. Guy, 2010, Nonlinear rheology of model filled elastomers, *J. Polym. Sci., Pt. B-Polym. Phys.* **48**, 2490-2496.

Phan-Thien, N., M. Newberry, and R.I. Tanner, 2000, Non-linear oscillatory flow of a soft solid-like viscoelastic material, *J. Non-Newton. Fluid Mech.* **92**, 67-80.

Poulos, A.S., J. Stellbrink, and G. Petekidis, 2013, Flow of concentrated solutions of starlike micelles under large-amplitude oscillatory shear, *Rheol. Acta* **52**, 785-800.

Princen, H.M., 1982, On the rheology of foams and highly concentrated emulsions, *J. Soc. Cosmet. Chem.* **33**, 371-371.

Ptaszek, P., 2015, A geometrical interpretation of large amplitude oscillatory shear (LAOS) in application to fresh food foams, *J. Food Eng.* **146**, 53-61.

Radhakrishnan, R. and S.M. Fielding, 2018, Shear banding in large amplitude oscillatory shear (LAOStrain and LAOStress) of soft glassy materials, *J. Rheol.* **62**, 559-576.

Renou, F., J. Stellbrink, and G. Petekidis, 2010, Yielding processes in a colloidal glass of soft star-like micelles under large amplitude oscillatory shear (LAOS), *J. Rheol.* **54**, 1219-1242.

Rogers, S.A., 2017, In search of physical meaning: Defining tran-

sient parameters for nonlinear viscoelasticity, *Rheol. Acta* **56**, 501-525.

Rogers, S.A., B.M. Erwin, D. Vlassopoulos, and M. Cloitre, 2011a, A sequence of physical processes determined and quantified in LAOS: Application to a yield stress fluid, *J. Rheol.* **55**, 435-458.

Rogers, S.A., B.M. Erwin, D. Vlassopoulos, and M. Cloitre, 2011b, Oscillatory yielding of a colloidal star glass, *J. Rheol.* **55**, 733-752.

Rogers, S.A. and M.P. Lettinga, 2012, A sequence of physical processes determined and quantified in large amplitude oscillatory shear (LAOS): Application to theoretical nonlinear models, *J. Rheol.* **56**, 1-25.

Rouyer, F., S. Cohen-Addad, and R. Höhler, 2005, Is the yield stress of aqueous foam a well-defined quantity?, *Colloids Surf. A-Physicochem. Eng. Asp.* **263**, 111-116.

Rouyer, F., S. Cohen-Addad, R. Höehler, P. Sollich, and S.M. Fielding, 2008, The large amplitude oscillatory strain response of aqueous foam: Strain localization and full stress Fourier spectrum, *Eur. Phys. J. E* **27**, 309-321.

Saint-Jalmes, A. and D.J. Durian, 1999, Vanishing elasticity for wet foams: equivalence with emulsions and role of polydispersity, *J. Rheol.* **43**, 1411-1422.

Stickel, J.J., J.S. Knutsen, and M.W. Liberatore, 2013, Response of elastoviscoplastic materials to large amplitude oscillatory shear flow in the parallel-plate and cylindrical-Couette geometries, *J. Rheol.* **57**, 1569-1596.

Sugimoto, M., Y. Suzuki, K. Hyun, K.H. Ahn, T. Ushioda, A. Nishioka, T. Taniguchi, and K. Koyama, 2006, Melt rheology of long-chain-branched polypropylenes, *Rheol. Acta* **46**, 33-44.

Tammaro, D., G. D'Avino, E. Di Maio, R. Pasquino, M.M. Villone, D. Gonzales, M. Groombridge, N. Grizzuti, and P.L. Maffettone, 2016, Validated modeling of bubble growth, impingement and retraction to predict cell-opening in thermoplastic foaming, *Chem. Eng. J.* **287**, 492-502.

Thompson, R.L., A.A. Alicke, and P.R. de Souza Mendes, 2015, Model-based material functions for SAOS and LAOS analyses, *J. Non-Newton. Fluid Mech.* **215**, 19-30.

van der Vaart, K., Y. Rahmani, R. Zargar, Z. Hu, D. Bonn, and P. Schall, 2013, Rheology of concentrated soft and hard-sphere suspensions, *J. Rheol.* **57**, 1195-1209.

Vishal, B. and P. Ghosh, 2018, Foaming in aqueous solutions of hexadecyltrimethylammonium bromide and silica nanoparticles: Measurement and analysis of rheological and interfacial properties, *J. Dispersion Sci. Technol.* **39**, 62-70.

Wagner, M.H., V.H. Rolón-Garrido, K. Hyun, and M. Wilhelm, 2011, Analysis of medium amplitude oscillatory shear data of entangled linear and model comb polymers, *J. Rheol.* **55**, 495-516.

Wapperom, P., A. Leygue, and R. Keunings, 2005, Numerical simulation of large amplitude oscillatory shear of a high-density polyethylene melt using the MSF model, *J. Non-Newton. Fluid Mech.* **130**, 63-76.

Wilhelm, M., 2002, Fourier-transform rheology, *Macromol. Mater. Eng.* **287**, 83-105.

Wilhelm, M., D. Maring, and H.W. Spiess, 1998, Fourier-transform rheology, *Rheol. Acta* **37**, 399-405.

Wilhelm, M., K. Reinheimer, and J. Kubel, 2012, Optimizing the sensitivity of FT-rheology to quantify and differentiate for the first time the nonlinear mechanical response of dispersed beer foams of light and dark beer, *Z. Phys. Chemie-Int. J. Res. Phys. Chem. Chem. Phys.* **226**, 547-567.

Yu, W., P. Wang, and C. Zhou, 2009, General stress decomposition in nonlinear oscillatory shear flow, *J. Rheol.* **53**, 215-238.